The effect of the Mo/W ratio on the catalytic properties of alumina supported hydrotreating catalysts prepared from mixed $SiMo_6W_6$ and $SiMo_9W_3$ heteropolyacids

A. Kokliukhin[a,b,d], M. Nikulshina[a,b], A. Mozhaev[a,c,d], C. Lancelot[b], P. Blanchard[b], O. Mentré[b], M. Marinova[e], C. Lamonier[b], and P. Nikulshin[a,c,d*]**

[a] *Samara State Technical University, 244, Molodogvardeyskaya st., Samara, 443100, Russia*

[b] *Univ. Lille, CNRS, Centrale Lille, ENSCL, Univ. Artois, UMR 8181 – UCCS – Unité de Catalyse et Chimie du Solide, F-59000 Lille, France*

[c] *All-Russia Research Institute of Oil Refining, 6/1 Aviamotornaya st., Moscow, 111116, Russia*

[d] *Gubkin Russian State University of Oil and Gas, Leninskiy Prospect 65, Moscow, 119991, Russia*

[e] *Univ. Lille, CNRS, INRA, Centrale Lille, ENSCL, Univ. Artois, FR 2638 - IMEC - Institut Michel-Eugène Chevreul, F-59000 Lille*

*Corresponding author at: Samara State Technical University, 244 Molodogvardiyskaya st., Samara 443100, Russia.

**Corresponding author at: Université Lille, UMR 8181 CNRS, UCCS, Villeneuve d'Ascq, France.

E-mail: p.a.nikulshin@gmail.com (Pavel Nikulshin), carole.lamonier@univ-lille.fr (Carole Lamonier).

Abstract

New mixed $H_4[SiMo_nW_{n-12}O_{40}]$ (n = 6 and 9) Keggin type heteropolyacids (HPAs) have been successfully synthesized, as confirmed by single-crystal XRD, Raman and IR spectroscopy analysis. The resulting polyoxometallates were used for preparation of hydrotreatment catalysts.

Mo(W)/Al_2O_3 catalysts were synthesized by incipient wetness impregnation of alumina support with water solutions of prepared mixed Keggin HPAs and corresponding counterparts based on mixture of monometallic $H_4[SiMo_{12}O_{40}]$ and $H_4[SiW_{12}O_{40}]$ HPAs. Oxidic catalysts were analyzed by Raman spectroscopy to determine the precursor structure after deposition. Catalysts in sulfided state were characterized by high-resolution transmission electron microscopy (HRTEM), high angle annular dark field imaging (HAADF) and X-ray photoelectron spectroscopy (XPS) and were tested in co-hydrotreating of dibenzothiophene (DBT) and naphthalene. The use of new mixed Keggin HPAs made it possible to obtain catalysts with mixed $MoWS_2$ active centers, which was confirmed by HAADF. Moreover, the Mo/(Mo+W) ratio has a direct effect on the structure of the active phase species. An ordered core-shell structure with Mo atoms in the core is maintained until the fraction of molybdenum in mixed MoW/Al_2O_3 catalyst exceeds 50%, where a more disordered structure is observed. Moreover, this Mo/(Mo+W) ratio of 0.5 is optimal to achieve a maximum catalytic activity. Indeed, the turnover frequencies (TOF) of the $MoWS_2$ edge centers with random atoms distribution in a cluster as in Mo_9W_3/Al_2O_3, was lower compared to that of Mo_6W_6/Al_2O_3 with core-shell structure.

Keywords: Hydrodesulfurization, hydrogenation, $SiMo_nW_{12-n}$ HPA, MoW mixed phase, DBT.

1. Introduction

The main problem of oil refining is the quality of the produced fuel, especially diesel and gasoline, as the world demand for these types of fuel increases every year, while environmental standards for diesel fuel have noticeably tightened [1,2]. According to the U.S. Energy Information Administration for 2018, global liquid fuels demand will increase more than 20% in 2050 [3], and the demand for motor fuels will reach 107 million barrels per day [4]. At the same time, the availability of light oil is coming to an end, and recently the world has been paying more and more attention to the use of heavy viscous oil sources, implying the use of more severe conditions in the

technology of hydrodesulfurization (HDS) (e.g., high temperature, high pressure, and high hydrogen consumption), which result in higher operating cost [5]. In this regard, the development of new catalytic systems for hydrogenation processes in order to produce ultra-pure motor fuels continues.

Increasingly, the attention of researchers is focused on the use of mixed Mo-W systems, promoted by Co or Ni, to create new highly active hydrotreating catalysts [6-12]. Raybaud and co-workers [6] have calculated that $NiMoWS_2$ phases are more active than NiMoS and NiWS ones, thanks to the optimal binding energy between sulfur and metal. Moreover, Hensen and co-workers [8] considered that depending on the sulfiding conditions two models of $MoWS_2$ mixed active phase can be formed: with random distribution of Mo and W atoms and a core-shell structure, where Mo is mainly located in the core, and W in the shell. It was found that $NiMo_{0.75}W_{0.25}/Al_2O_3$ catalyst with a random distribution of Mo and W atoms in mixed $MoWS_2$ slabs was formed in liquid phase sulfidation conditions and was more active in the gas oil hydrotreatment compared to $NiMo/Al_2O_3$. Mixed $MoWS_2$ slabs with a core-shell structure were formed in gas sulfidation conditions and their testing in thiophene HDS did not show any synergistic effect.

Various types of mixed MoW systems can be found in the literature, which preparation mostly involves traditional precursors of the active phase, such as ammonium heptamolybdate (AHM), ammonium paratungstate (APT), ammonium metatungstate (AMT) and ammonium tungstate. [10-12]. Heteropolycompounds, such as Keggin and Keggin-derivated heteropolymolybdate and heteropolytungstate structures, can be used as starting oxidic precursor for highly active hydrotreating catalysts [13-17]. We have previously proposed a new method to synthetize (Ni)MoW catalysts using mixed $H_4[SiMo_1W_{11}O_{40}]$ and $H_4[SiMo_3W_9O_{40}]$ heteropolyacids (HPA), allowing to introduce both Mo and W metals in a catalyst from a single molecular precursor [18]. It was found that such catalysts are more efficient than their counterparts obtained from a mixture of monometallic HPAs with the same Mo/(Mo+W) ratio, which was related to the formation of a mixed $MoWS_2$ phase when using mixed HPA as precursor [19,20].

Moreover, it was found that when increasing the Mo/(Mo+W) atomic ratio from 0.08 to 0.25, the catalytic activity also increases. However, a synthesis methodology has only been published for HPAs with Mo/W molar ratio equal to 1/11 and 3/9 [19]. In this work, we have successfully synthesized new Keggin HPAs with a molar ratio equal to 6/6 and 9/3, which were characterized by XRD, Raman and IR spectroscopy. The purpose of this study was to determine the effect of the increase of the Mo/(Mo+W) molar ratio on the formation of the mixed $MoWS_2$ active phase and subsequently on the catalytic activity in dibenzothiophene (DBT) HDS and naphthalene hydrogenation (HYD). The performance in the hydrotreating reactions of DBT and naphthalene was evaluated and compared to that of reference catalysts obtained from a mixture of two monometallic Mo and W based HPAs with the same Mo/(Mo+W) ratio. All catalysts were activated under gas phase sulfidation under a flow of H_2S/H_2 (10 vol. %) and characterized by XPS, HRTEM and HAADF.

2. Experimental

2.1 Synthesis of mixed $H_4[SiMo_nW_{12-n}O_{40}]$ heteropolyacids (HPAs) (n = 1, 3, 6, 9)

Mixed α-$H_4[SiMo_1W_{11}O_{40}]$ and β-$H_4[SiMo_3W_9O_{40}]$ heteropolyacids (hereafter $SiMo_1W_{11}$ and $SiMo_3W_9$) have been synthesized from their corresponding mixed potassium salt starting from mono(tri)-vacant heteropolytungstates according to previous reports [19].

Two new $SiMo_nW_{12-n}$ HPAs with Mo/W molar ratio equal to 6/6 and 9/3 were synthesized by the same method using monometallic $H_4[SiMo_{12}O_{40}]$ ($SiMo_{12}$) and $H_4[SiW_{12}O_{40}]$ (SiW_{12}) HPAs as starting materials:

- for Mo/W = 6/6: 4.12 g of $SiMo_{12}$ and 6.21 g of SiW_{12} acids dissolved in 40 ml of distilled water;
- for Mo/W = 9/3: 6.62 g of $SiMo_{12}$ and 3.44 g of SiW_{12} acids dissolved in 48 ml of distilled water.

Yellow solutions were obtained in both cases. The acid solutions were heated to 80°C and kept for 1 h. After that, potassium hydroxide was added to each solution in small portions. until pH reaches 4. After the addition of alkali, the solution became slightly greenish. Both solutions

were boiled for another 30 min at 80℃ and then cooled to room temperature. It was noticed that the mixed corresponding acid was sufficiently stable to be crystallized from aqueous solution by using the "etherate" method [21]. The extraction and the crystallization were carried out according to the procedure described previously [19]. The elemental composition and structures of the mixed heteropolyacids were confirmed by XRD, IR-, and Raman spectroscopy. The crystal data and the structure refinement parameters for the obtained crystals are given in Table 1.

2.2 Preparation of the supported oxidic precursors

The catalysts with surface density of the metals d(Mo + W) equal to 3.9 at nm^{-2} were prepared by incipient wetness impregnation of alumina support [γ-Al_2O_3 (Norton), specific area: 240 m^2 g^{-1}, pore volume: 0.9 mL g^{-1}] with the aforementioned impregnating solutions. The bimetallic Mo_nW_{12-n} catalysts were prepared by using corresponding mixed and $H_4[SiMo_nW_{n-12}O_{40}]$ HPAs and will be referred to as Mo_nW_{12-n}/Al_2O_3. Reference catalysts were also prepared using the impregnating solutions obtained by mixing $SiMo_{12}$ and $SiMo_{12}$ in an aqueous solution with the same Mo/W ratio corresponding to the mixed HPAs and were denoted as Mo_n+W_{12-n}/Al_2O_3. The oxidic catalyst precursors after maturation were dried at 60°C (4 h) 80°C (2 h) and 100°C (4 h) in air atmosphere without further calcination. The chemical compositions of the prepared catalysts are given in Table 2. The oxidic catalysts were analyzed by Raman spectroscopy.

2.3. Characterization of the solids

2.3.1 Raman and IR- spectroscopy

The Raman spectra of the samples were recorded at RT using an Infinity XY Horiba Jobin-Yvon Raman microprobe equipped with a photodiode array detector. The excitation laser source was the 532.16 nm line of a Nd-YAG laser. The wavenumber accuracy was 4 cm^{-1}. IR spectra of $H_4[SiMo_nW_{n-12}O_{40}]$ HPAs (as KBr pellets) (400–4000 cm^{-1}) were measured on a Shimadzu IR Prestige-21 FT-IR spectrophotometer.

2.3.2 Single-crystal X-ray diffraction (XRD)

Single crystal XRD data for $H_4[SiMo_6W_6O_{40}]\cdot 36H_2O$ and $H_4[SiMo_9W_3O_{40}]\cdot 36H_2O$ have been collected using a Bruker Apex Duo diffractometer with a Mo-IμS microfocus tube (λ=0.71073 Å). The intensity data have been extracted and corrected from Lorentz Polarization using the program SAINT-Plus 8.27b [22]. Multiscan absorption correction was applied using SADABS [23]. The structure was solved using Superflip [24] and refined using Jana 2006 [25]. Specificities for each collection and refinement are given in the crystal structure dedicated sections.

2.4 Textural characteristics of the oxidic precursors

The textural characteristics of the catalysts were measured on a Quantachrome Autosorb-1 adsorption porosimeter by low-temperature nitrogen adsorption at 77 K. Before analysis, the samples were outgassed under vacuum (< 10^{-1} Pa) at 300°C for 3 h. The specific surface area (SSA) was calculated using the Brunauer-Emmett-Teller method at relative partial pressures (P/P_0) ranging from 0.05 to 0.3. Total pore volume (at P/P_0 of 0.99) and pore size distribution were obtained using the desorption curve and the Barret-Joyner-Halenda model.

2.5 Characterization of the sulfided catalysts

2.5.1 High resolution high-angle annular dark-field scanning transmission electron microscopy (HR HAADF-STEM)

HAADF-STEM analyses have been performed using a FEG TEM/STEM system (Titan Themis FEI) operated at 300 kV, equipped with a monochromator and a probe Cs corrector. For HAADF acquisition, the spot size was 9 (probe size of the order of 500 pm) with a screen current of ~50 pA and collection angles for the HAADF detector of ~50 and ~200 mrad, respectively. The probe semi-convergence angle has been 21 mrad. All samples were ground under an inert atmosphere. In order to avoid contamination, the samples have been deposited in the form of dry powder, without solvents, on cupper grids with the lacey carbon film.

2.5.2 High-resolution transmission electron microscopy (HRTEM)

HRTEM was carried out using a Tecnai G2 20 electron microscope with LaB_6 filament with a 0.19 nm lattice-fringe resolution and an accelerating voltage of 200 kV. The samples were dispersed in ethanol. The suspension was collected on carbon films supported on copper grids and 10 – 15 representative micrographs were obtained for each catalyst in high–resolution mode. Typically, the length and the stacking of at least 500 slabs were measured for each catalyst. ImageJ free software developed for direct qualitative analysis of images. The distribution in length and the stacking of the slabs was determined. To measure the extent of the Mo(W)S_2 dispersion, the average fraction of Mo(W) atoms at the Mo(W)S_2 edge surface (D) was calculated, assuming that the Mo(W)S_2 slabs were perfect hexagons [26]. Mo(W)S_2 dispersion (D) was statistically evaluated by dividing the total number of Mo(W) atoms at the edge surface (W_e), including corner sites (W_c), by the total number of Mo(W) atoms (W_T) using the slab sizes measured in the TEM micrographs:

$$D = \frac{W_e + W_c}{W_T} = \frac{\sum_{i=1..t} 6n_i - 6}{\sum_{i=1..t} 3n_i^2 - 3n_i + 1}, \quad (1)$$

where n_i is the number of Mo(W) atoms along one side of the Mo(W)S_2 slab, as determined by its length, and t is the total number of slabs in the TEM micrograph.

The number of slabs per stack was determined to obtain the average stacking degree ($\overline{N}$):

$$\overline{N} = \frac{\sum_{i=1..t} n_i N_i}{\sum_{i=1..t} n}, \quad (2)$$

where n_i is the number of stacks in N_i layers.

2.5.3 X-ray photoelectron spectroscopy (XPS)

The sulfided catalyst samples were analysed by XPS. The spectra were recorded on a Kratos Axis Ultra DLD spectrometer using a monochromatic Al Kα source (hν = 1486.6 eV, 150 W). The

samples were mounted on a holder using double-sided adhesive tape. For the non-conductive samples, the Kratos charge neutraliser system was used and the spectra were charge-corrected to provide the C 1s spectral component of adventitious carbon (C–C, C–H) at 284.8 eV. In addition to the survey photoelectron spectra, narrow spectral regions (Al 2p, S 2p, Mo 3d, W 4f, C 1s and O 1s) were recorded. The binding energy (BE) scale of the spectrometer was preliminarily calibrated using the position of the peaks for the Au $4f_{7/2}$ (83.96 eV) and Cu $2p_{3/2}$ (932.62 eV) core levels of pure metallic gold and copper. The pass energy of the analyser was 160 eV for the survey spectra and 40 eV for the narrow scans. The individual spectral regions were analysed to determine the BE of the peaks, identify the chemical state of the elements and calculate the relative ratios of the elements on the catalyst surface.

The collected spectra were analysed using the CasaXPS software program (Version 2.3.16) after applying a Shirley background subtraction. Gaussian (30%) – Lorentzian (70%) peaks were used for spectra decomposition. All XPS spectra were carefully decomposed according to previous works [20,27,28].

2.6 Evaluation of catalytic activities

The catalytic activity was determined in a flow high-pressure fixed-bed microreactor. Prior to testing, the catalysts were sulfided in a flow of H_2S/H_2 (10 vol. %) at atmospheric pressure and 400 °C for 2 h. 0.4 g of catalyst (0.25 – 0.50 mm) was diluted with of low-surface-area sieved carborundum (0.2–0.4 mm) in a ratio of one to one and placed in isothermal zone of the reactor. Catalysts were tested under the following conditions: 320°C, 3.0 MPa of hydrogen, 10 h^{-1} liquid hourly space velocity (LHSV) and a 500 NL L^{-1} volume ratio of hydrogen to feed. For evaluation of HDS and hydrogenation performances, a mixture of DBT (1000 ppm S), naphthalene (3 wt. %), hexadecane (as an internal standard, 1 wt. %) and toluene (as a solvent) was used. The liquid product compositions of the samples collected every hour were determined using a Crystall-5000 Gas Chromatograph equipped with a 30 m OV-101 column.

The products of reactions were identified by GC/MS analysis using a Finnigan Trace DSQ. All catalysts exhibited stable performance, achieving a steady state after 7 – 10 h.

The rate constants of the pseudo-first-order reactions of the DBT HDS and naphthalene HYD were determined using the equations presented in our previous works [20,27].

3. Results

3.1 Characterization of the solids

3.1.1 IR- and Raman spectroscopy of Mo_nW_{12-n} HPAs

IR and Raman spectra of $H_4[SiMo_nW_{12-n}O_{40}]$ HPAs (with n = 1, 3, 6 and 9) are presented in Fig. 1 and Fig. 2, respectively. IR and Raman spectra of monometallic and mixed HPAs are very close and present the typical peaks of Keggin structure.

In IR spectra, characteristic peaks assigned to the Keggin structure are observed [29,30], at 913-930 and 957-982 cm^{-1} for Si-O and Mo(W)-O_t vibrations stretching mode respectively. together with lines at 867-882 and 773-780 cm^{-1} corresponding to Mo(W)-O_b-Mo(W) and Mo(W)-O_c-Mo(W) vibrations. The increase of the Mo content in $SiMo_nW_{12-n}O_{40}^{4-}$ is reflected by a slight increased shift to the lower wavenumbers for Mo(W)-O_t and Mo(W)-O_b-Mo(W) lines. All Raman spectra (Fig. 2) are dominated by a main peak corresponding to symmetric ν_s(Mo(W)-O_t) terminal vibration [29,31,32]. For the high W content mixed HPA, $SiMo_1W_{11}$ and $SiMo_3W_9$ HPAs this position of this line (1005 cm^{-1}) is similar to that observed for $SiW_{12}O_{40}$ while a more important shift towards low wavenumbers is observed with the increase of Mo [33]. An important difference is observed for vibrations ν_s(W-O_c-W) and ν_s(Mo-O_c-Mo), which correspond to peaks at 552 and 638 cm^{-1}. In the case of spectra for mixed HPAs, a weak peak is observed, which lies between 552 and 638 cm^{-1}, which may indicate the presence of both vibrations and possibly the presence of ν_s(Mo-O_c-W) vibrations.

Both Raman and IR analyses seem to be in agreement with the formation of mixed Keggin structure for the new synthesized mixed $SiMo_6W_6$ and $SiMo_9W_3$heteropolyacids. Nevertheless, in

order to rebut the formation of separate monometallic HPA, single crystal XRD has been performed for characterization.

3.1.2 Single-crystal XRD

The experimental data collection and refinement results are listed in Table 1. Both HPA compounds $SiMo_6W_6$ and $SiMo_9W_3$ are isomorphs and crystallize in the tetragonal space group P -42_1c. The number of hydration water molecules determined during the structural refinement correspond to 36 molecules per $H_4[SiMo_nW_{12-n}O_{40}]$ cluster for the two compounds in agreement with their nearly identical refined lattice parameters. Before going into the structural details, one should note the poor stability of the crystals in air at ambient temperature, even more pronounced for the $H_4[SiMo_6W_6O_{40}]$, polycation for which a single crystal had to be isolated very rapidly and collected at 100K in a cold nitrogen flow to prevent from degradation by moisture into an amorphous solid. For the $H_4[SiMo_9W_3O_{40}]$ hydrate a simple protection of the crystals by vacuum grease allows full data collection at room temperature. The two crystal structures are similar and show a distribution of HPA (two per unit cell) separate by ca.12.75Å (d(Si-Si)) (Fig. 3b) surrounded by water molecules. These latter have been located on difference-Fourier maps and show very high thermal parameters which reflect local disorder/off-centering due the proton and Mo/W disorder on the counter molecules (Fig. 3). Residual peaks subsist at the end of the refinement which picture partial water positions but have not been taken into account due to even higher vibrations. Finally, 36 water molecules were found per formula unit in both cases. For both compounds, the Mo/W occupancy and the scale factor parameters are strongly correlated which complicate the determination of the real Mo/W ratio during refinement. However, it was checked that fixing the ratio to the preparation stoichiometry leads to best R% values together with most reasonable thermal parameters for all atoms. No evidence was found that Mo/W are ordered by three independent positions offered in the crystal structure, contrarily to what occasionally occurs [19].

Single crystal XRD of $SiMo_6W_6$ and $SiMo_9W_3$ HPA allows to conclude that mixed heteropolyanions containing together both W and Mo atoms were formed.

3.2 Raman spectroscopy of supported oxidic precursors

To better understand the behavior of these HPAs after deposition on the support, the Raman analysis was performed and obtained Raman spectra of the oxidic catalysts are shown in Fig. 4. For comparison purposes, Raman spectra of the oxidic precursors prepared from a mixture of monometallic HPA $SiMo_{12}$ and SiW_{12} are also reported in Fig. 4. For precursors prepared from a mixture of HPA, the main Raman line observed around 970 cm^{-1} and corresponding to Mo(W)-O terminal vibrations presents an important shoulder at 950 cm^{-1}, increasing with Mo content, witnessing to the presence of Keggin entities with other species. Mo_{12}/Al_2O_3 presents in fact the Raman spectrum of $AlMo_6$ Anderson species in agreement with results previously reported [34,35]. For oxidic catalysts prepared from a mixture of SiW_{12} and $SiMo_{12}$ HPA, the shoulder noticed at 950 cm^{-1} is then due to the $AlMo_6$ formation from instable $SiMo_{12}$ species when deposited on alumina due to the "buffer effect" of alumina and Al^{3+} extraction from the support [36,37]. For the corresponding catalysts prepared from mixed HPAs ($SiMo_9W_3$, $SiMo_6W_6$ and $SiMo_3W_9$) the shoulder is not observed. It is in agreement with the use of a mixed $SiMo_nW_{12-n}$ HPA more stable on alumina support than the $SiMo_{12}$ one. A shift of the main peaks is also observed with the increase of molybdenum content, as was previously noted on Raman and IR spectra of bulk HPAs. Moreover, analysis of the low Raman shift region (below 230 cm^{-1}) shows lines similar in shape and position for the bulk and the corresponding Keggin W-based HPA catalysts [29], except for Mo_9W_3/Al_2O_3 and Mo_9+W_3/Al_2O_3 ones, in which the proportion of molybdenum is much higher. In this case, all peaks are shifted to the low wavenumbers. New Raman lines of Mo_{12}/Al_2O_3 and Mo_9+W_3/Al_2O_3 are clearly observed at 550, 350 and 215 cm^{-1}, which are unambiguously assigned to the formation of the well-known $AlMo_6O_{24}H_6^{3-}$ Anderson heteropolyanion species. As already noted, for the W-based catalysts, after drying, a shift from 1007 to 977 cm^{-1} of the main line ($W\text{-}O_t$ vibration) towards lower wavenumbers due to interaction

with the support is observed [19]. According to the obtained spectral data, it can be assumed that the mixed MoW structure is preserved even after maturation and drying.

3.3 Characterization of supported Mo(W)/Al_2O_3 sulfide catalysts

3.3.1 HRTEM

All catalysts were characterized by HRTEM to obtain more information about the dispersion of Mo(W)S_2 active phase. The HRTEM micrographs are shown in Fig. 5. The observed black slabs correspond to Mo(W)S_2 crystallites with 0.65 nm interplanar distances. For each catalyst, the distributions in stacking degree and length of the Mo(W)S_2 slabs were determined, as well as the corresponding average values, presented in Table 3. The length was measured for each sample using. The average particle length and stacking number ranged from 3.6 to 4.2 nm and from 1.2 to 2.3, respectively. The highest number stacking value corresponds to Mo_3+W_9/Al_2O_3 catalyst. The increase in molybdenum percentage led to a simultaneous decrease the stacking number of Mo(W)S_2 active phase particles (from 2.3 to 1.2) for Mo_n+W_{n-12}/Al_2O_3 catalysts. The dispersion of the active phase varies between 0.28 and 0.34. Moreover, the dispersion of the active phase of mixed Mo_nW_{12-n} catalysts decreased from 0.34 to 0.29 with increasing Mo/W ratio from 3/9 to 9/3, while it increased from 0.29 to 0.32 for the ones based on the mixture HPAs counterparts.

3.3.2 HAADF

Typical HAADF images of sulfided Mo_3W_9/Al_2O_3, Mo_6W_6/Al_2O_3 and Mo_9W_3/Al_2O_3 catalysts are presented in Fig. 6. One advantage of HAADF is that it allows to discriminate between Mo and W atoms due to their difference in atomic number (W atoms appear thus brighter than Mo ones), as already evidenced in a previous study [18]. The intensity in HAADF images, for a given thickness and density and depending on the collection angles, is a function of the atomic number. Therefore, W atoms appear brighter than Mo atoms in the HAADF images. The most attention was paid to the monolayer particles and their structure. In the case of the Mo_6W_6/Al_2O_3 sample, as well as for the Mo_3W_9/Al_2O_3 [20], mixed slabs are formed in which the molybdenum

atoms are concentrated in a core, and the tungsten atoms are located in a shell. At the same time, tungsten atoms are localized at the edges of the slab and formed a rim around molybdenum atoms. The Mo_9W_3/Al_2O_3 sample was characterized by a disordered structure of the active phase, where the two-dimensional foils can be represented as MoS_2 particles with small inclusions of W atoms. Perhaps this can be explained by the different kinetics of sulfidation of Mo and W atoms and an excess of the former in the structure. According to the data obtained by HAADF imaging, it can be concluded that the structure of mixed $MoWS_2$ particles depends on the ratio of molybdenum and tungsten in the structure. Therefore, when the content of Mo increases from 50 (in Mo_6W_6/Al_2O_3 catalyst) to 75 at % (in Mo_9W_3/Al_2O_3), a transition occurs from an ordered core-shell structure to a disordered structure in which tungsten atoms are randomly located.

3.3.3 XPS spectroscopy

Information about the composition of sulfide particles on the surface of the synthesized catalysts was obtained in detail by XPS. The XPS spectra of Mo_nW_{12-n}/Al_2O_3 and Mo_n+W_{12-n}/Al_2O_3 were decomposed thanks to previous works [20,27,28] using the appropriate oxide and sulfided references as supported monometallic catalysts for example (Fig. 7). The Mo3d spectra contain three doublets: 229.0 eV and 232.0 eV correspond to $Mo3d_{5/2}$ and $Mo3d_{3/2}$ of Mo^{4+} (MoS_2 species), doublet at about 230.0 and 233.5 eV is related to Mo^{5+} (MoO_xS_y species) and doublet at 232.5 and 235.7 eV is associated with Mo^{6+} oxide species.

The W 4f spectra contain three W 4f doublets: the doublet with binding energies (BE) at 32.1 and 34.3 eV is associated to $W4f_{7/2}$ and $W4f_{5/2}$ of W^{4+} species of the WS_2 phase, the doublet with binding energies at 33.0 and 35.2 eV to W^{5+} species of a WS_xO_y oxysulfide species, and finally the doublet with binding energies at 36.0 and 37.9 eV correlated with W^{6+} oxide species. It should also be kept in mind that the $W5p_{3/2}$ and Mo4p ranges (non splitted level) overlap the W4f levels. The contributions of these peaks were excluded when calculating the true content of W4f fractions. All the constraints between BE, FWHM and the peak areas of Mo4p and $Mo3d_{3/2}$ were determined experimentally by XPS analysis of the Mo_{12}/Al_2O_3 oxide catalyst.

The results of the XPS decomposition for the metal fractions of molybdenum and tungsten species of the sulfided Mo_nW_{12-n}/Al_2O_3 and Mo_n+W_{12-n}/Al_2O_3 are reported in Table 4. In all bimetallic catalysts, the sulfidation degree of molybdenum was higher than 80 rel. %. The highest values (91 rel. %) of the degree of sulfidation correspond to Mo_6W_6/Al_2O_3 and Mo_9W_3/Al_2O_3 catalysts. Moreover, the Mo_9W_3/Al_2O_3 catalyst also corresponds to the highest degree of tungsten sulfidation equal to 85 rel. %. Replacing a quarter of the Mo atoms with W made it possible to increase the sulfidation degree by more than 20 rel. % compared to Mo_{12}/Al_2O_3 catalyst. It should also be noted that the sulfidation degree of Mo in mixed Mo_nW_{12-n}/Al_2O_3 catalysts was higher than in bimetallic Mo_n+W_{12-n}/Al_2O_3 samples prepared from mixture of HPAs. Sulfidation of molybdenum oxide occurs at lower temperatures, while tungsten oxide sulfides at higher temperatures due to thermodynamics and lower reactivity [38]. As already noted, sulfidation of MoW catalysts begins with the formation of MoS_2 nuclei, which contribute to the activation of H_2S, which allows increasing the degree of sulfidation of WO_3 and raising the number of active sites [18]. Moreover, this effect is enhanced by the use of mixed HPAs as oxide precursors of the active phase, which have shown in previous works [18,20]. It can be explained by the proximity of Mo and W atoms in the structure. It should also be noted that an increase in the molybdenum content contributed to an increase in the degree of sulfidation of both metals in mixed Mo_nW_{12-n}/Al_2O_3 catalysts.

It was assumed that no mixed crystallites are formed during the sulfidation process when calculating the number of edge sites (Table 4). Only the mass percentage of MoS_2 calculated from the XPS data and dispersion were taken into account. This made it possible to estimate in a general way the number of active centers without taking into account their nature. Since the dispersion of the active phase for all catalysts was approximately equal, the key effect on the number of edge centers was exerted only by the sulfidation degree of metals. An increase in the molybdenum content leads to an increase in the content of edge sites for both types of catalysts due to the high degree of sulfidation of both metals. However, it should be noted that degree of metal sulfidation

in monometallic Mo_{12}/Al_2O_3 and W_{12}/Al_2O_3 catalysts is less than that of bimetallic MoW/Al_2O_3 samples, which can be explained by the absence of a synergistic effect between Mo and W, described in detail by Nikulshina et al [39].

3.4 Catalytic activities

The catalytic activities of the sulfided Mo_nW_{12-n}/Al_2O_3 and Mo_n+W_{12-n}/Al_2O_3 catalysts in co-HDT of DBT and naphthalene are presented in Table 5. The reactants conversions varied in a wide range, from 20.6 to 61.3% for HDS of DBT and from 23.8 to 57.3% for HYD of naphthalene over all prepared catalysts. The W_{12}/Al_2O_3 sample demonstrated the lowest activities in DBT HDS (22.2 %) and in naphthalene HYD (23.8 %). All Mo_n+W_{12-n}/Al_2O_3 catalysts prepared from two monometallic HPA demonstrated a lower activity than the monometallic Mo_{12}/Al_2O_3 sample in HDS DBT. It was noted that with an increase in the Mo/W ratio of 0.33 or more, an increase in catalytic activity occurs in both HDS and HYD reactions (Fig. 8). An increase in Mo/(Mo+W) molar ratio above 0.5 contributes to a decrease in catalytic activity. The highest effect was observed for the Mo_6W_6/Al_2O_3 sample which is more than 15% active in DBT HDS and naphthalene HYD than analogues prepared from a mixture of monometallic heteropolyacids with the same molar ratio.

4. Discussion

All analyzed catalysts have similar textural characteristics (Table 2) and dispersion of the active phase particles (Table 3). It should be noted that the replacement of one atom of tungsten by molybdenum atom is a sharp increase an average stacking number (Fig. 9) due to the change of the metal sulfidation rate, which is also reflected in the XPS results. Further, with an increase in the molybdenum content in the catalyst, a gradual decrease in the number of layers occurs, regardless of the type of oxide precursor of the active phase. This can be explained by the fact that there is an interaction between the molybdenum oxide particles and the surface of support [40,41], which were observed on the Raman spectra. This leads to the formation of particles with fewer layers in the package, which is also consistent with literature [42].

As we can see from Fig. 8, the catalytic activity increases with the molybdenum content and reaches a maximum with a Mo/(Mo+W) ratio of 0.5. Similar dependencies for CoMoW/SBA-15 catalysts prepared from AHT, AMT and cobalt nitrate hexahydrate were published by Huirache-Acuña et al [43]. It was reported that the maximum activity in DBT HDS was achieved with a molar ratio of Mo/(Mo+W) equal to 0.6, which almost corresponds to the result obtained in the work. Wang et al. [44], using the density functional theory (DFT) calculations, found that the 50% substitution of Mo by W in unsupported mixed $MoWS_2$ catalysts shows the best hydrogen activation because of the reduction of H adsorption free energy and facilitation of charge transfer. Further increase in the concentration of molybdenum led to a slight decrease in activity for both types of catalysts (Fig. 8). It follows from this case, the catalytic activity is primarily affected by the ratio of metals of the $Mo(W)S_2$ active phase.

Improved catalytic properties both in the HDS and HYD reactions were performed on catalysts synthesized from mixed $SiMo_nW_{12-n}$HPAs for all studied Mo/W ratios. These observations allowed us to conclude that the origin of the catalytic improvement is not only due to the simultaneous presence of Mo together with W, but also arises from the close interaction of both metals in the mixed oxide precursor. As previously described, mixed slabs are formed mainly in samples that have been synthesized from mixed HPAs [18,20] and it was confirmed by the HAADF. Haandel et al. [8] also described mixed structures for Ni-Mo-W catalysts prepared from conventional precursors (AHM and AMT) and sulfided under gas phase sulfidation. It is assumed that the structure of the mixed active phase depends on the type of sulfidation: the random arrangement of metal atoms during sulfidation at high pressure and the core-shell structure during gas-phase sulfidation at low pressure [8]. Earlier, a random-structure was reported to form on a catalyst based on mixed $SiMo_3W_9$HPA during liquid-phase sulfidation, while a core-shell structure is formed during gas-phase sulfidation [20]. However, from the present study, the atomic ratio in oxidic precursor can affect the structure of mixed centers. The core-shell structure is retained for

a molar Mo/(Mo+W) ratio of 0.25 and 0.5, while with ratio equal to 0.75, a random structure prevails, which also explains a slight decrease in catalytic activity of Mo_9W_3/Al_2O_3.catalyst.

For better understanding of the catalytic properties of the Mo(W)S_2 active phase species the turnover frequencies (TOF, s^{-1}) normalized on edge sites of slabs for the HDS of DBT and HYD of naphthalene were calculated using the following equations:

$$TOF_{\mathrm{HDS}} = \frac{F_{\mathrm{DBT}} \cdot x_{\mathrm{DBT}}}{W \cdot \left(\frac{C_{\mathrm{WS_2}}}{Ar_W} + \frac{C_{\mathrm{MoS_2}}}{Ar_{Mo}} \right) \cdot D \cdot 3600} \text{ and } TOF_{\mathrm{HYD}} = \frac{F_{\mathrm{Naph}} \cdot x_{\mathrm{Naph}}}{W \cdot \left(\frac{C_{\mathrm{WS_2}}}{Ar_W} + \frac{C_{\mathrm{MoS_2}}}{Ar_{Mo}} \right) \cdot D \cdot 3600}, \quad (3)$$

where F_{DBT} and F_{Napl} are the reactant flow (mol h^{-1}); x_{DBT} and x_{Napl} are the conversions (%) of DBT and naphthalene, respectively; W is the weight of the catalyst (g); $C_{\mathrm{WS_2}}$ and $C_{\mathrm{MoS_2}}$ are the effective content of W and Mo, respectively, in $Mo_nW_{12-n}S_2$ species (wt. %); D is the dispersion of $Mo_nW_{12-n}S_2$ species; Ar_W and Ar_{Mo} are the standard atomic weight of tungsten (183.9 g/mol) and molybdenum (95.9 g/mol), respectively.

Fig. 10 shows the dependence of the TOF number on the Mo/(Mo+W) molar ratio for DBT HDS and naphthalene HYD. It is seen that the TOF number linearly increase with increasing molybdenum content in the mixture of Mo_n+W_{12-n} catalysts. This dependence is fully consistent with the calculated linear dependence (triangular markers) of the additive quantities, which were calculated using the values for monometallic Mo_{12}/Al_2O_3 and W_{12}/Al_2O_3. The TOF number for both reactions were significantly higher for mixed MoW/Al_2O_3 catalysts than for reference samples prepared from a mechanical mixture of monometallic HPAs, which also indicates that in the first case highly active mixed $MoWS_2$ centers are formed. All mixed MoW/Al_2O_3 samples have approximately equal TOF number (Fig 10), which simply indicates the similar "mixed" nature of the active centers. A significant growth in conversion for the Mo_6W_6/Al_2O_3 sample can be explained by a high content of edge active sites in the crystallites (Fig 11). It is also worth noting that with an increase in the molybdenum content of more than 50% in mixed Mo_nW_{12-}

$_n/Al_2O_3$ catalysts leads to a decrease in total catalytic activity correlated with a decrease of number of mixed sites due to the change in the Mo/W atomic ratio from a equimolar value and transition of the core-shell structure to a disordered one, which is also evidenced by the HAADF images. Nevertheless, the TOF number for the reference samples is significantly inferior to the additive quantities. This can be caused by the partial mechanical shielding of the active sites located on edges of separate MoS_2 and WS_2 crystallites.

Mo_9W_3/Al_2O_3 catalyst is significantly inferior to additive TOF number and fits linearly with catalysts prepared from a mechanical mixture (Fig. 10), which is consistent with the data presented by Hensen and co-workers [8]. Earlier, the effect of the Mo/(Mo+W) ratio on the formation of the mixed $MoWS_2$ phase under gas phase sulfidation was not studied, as well as the determination of the effect structure of mixed $MoWS_2$ particles on the catalytic activity. In this work, we can conclude that the random arrangement of atoms has a negative effect on catalytic activity, which is also consistent with the results of the effect of the type of sulfidation on the formation of a mixed active phase [20]. Moreover, the disordered structure of the Mo_9W_3/Al_2O_3 catalyst has a lower hydrogenation activity, which is also confirmed by the HYD/DDS selectivity in DBT HDS and the reaction rate constant of the naphthalene HYD and thus contradicting the data of the literature [8]. However, the authors [8] did not determine the catalytic activity in the DBT HDS for catalysts with a core-shell active phase structure, which makes it difficult to direct compare the data presented in our work. Each structure was tested in only one reaction: the core-shell structure – for the thiophene HDS reaction, the random structure for the DBT HDS reaction. But in both cases, no synergistic effect was found.

In the present study, it was shown that catalytic activity has a volcanic dependence on the ratio Mo/(Mo + W), with a maximum at 0.5 (Fig. 12), which is consistent with published works [44]. As mentioned earlier, the active sites forming from mixed Mo_nW_{12-n}HPAs with different Mo/(Mo + W) ratios have the same "mixed" nature (Fig. 10). Thus, the use of mixed Mo_nW_{12-n}HPAs with an equivalent molar ratio of active metals allows the formation of a maximum number

of mixed active sites on the catalyst surface. The decrease in the number of accessible active centers at a higher Mo/W ratio = 9/3 may be resulted from the blocking of tungsten atoms by molybdenum once during catalyst sulfidation. It is known [8,39] that a small fraction of tungsten oxide can undergo sulfidation at low temperatures and not all Mo atoms are in sulfides before beginning of the sulfidation of tungsten.

5. Conclusions

A new simplified method for the synthesis of mixed Keggin's HPAs with the molar Mo/(Mo+W) ratio equal to 0.5 and 0.75 through single-stage preparation has been proposed. The structure of the obtained compounds was confirmed by Raman, IR and single-XRD methods. $SiMo_6W_6$ and $SiMo_9W_3$ catalysts supported on alumina were more active in DBT HDS and naphthalene HYD reactions than their Mo+W references prepared using their monometallic counterparts, due to the formation of a mixed active phase, as observed by HAADF. It was found that the structure of active phase depends not only on the type of sulfidation which was reported previously [8,20], but also on the atomic Mo/(Mo+W) ratio in oxidic precursor used. An increase in this ratio from 0.25 to 0.5 allowed a significant increase in the number of edge sites more than 15% for Mo_6W_6/Al_2O_3 compared to Mo_3W_9/Al_2O_3 and more than 30% compared to monometallic Mo_{12}/Al_2O_3 (Fig 11).

The maximum conversion of reagents in the studied reactions was achieved with a ratio of Mo to W equal to 1: 1 for both types of Mo_6W_6/Al_2O_3 and Mo_6+W_6/Al_2O_3 catalysts. Mixed Mo_6W_6/Al_2O_3 sample was more active than a mixture reference due to formation of highly active mixed $MoWS_2$ slabs with core-shell structure, which was also evidenced by the HAADF images. This arrangement of atoms in the structure provides a significantly higher HYD activity, as evidenced by a higher $S_{HYD/DDS}$ selectivity of DBS HDS and HYD naphthalene than catalysts with a random distribution of atoms in slabs.

Conflicts of interest

There are no conflicts to declare.

Acknowledgments

The authors thank Russian Science Foundation for financial support of instrumental and theoretical part of the investigation by Grant No. 17-73-20386. The research was financially supported by the Ministry of Foreign Affairs and International Development (France), the Ministry of National Education, Higher Education and Research (France) in the framework of PHC Kolmogorov PHC 2017–2019. The TEM facility in Lille (France) is supported by the Conseil Regional du Nord-Pas de Calais and the European Regional Development Fund (ERDF).

The authors thank the Chevreul Institute (FR 2638) for its help in the development of this work. Chevreul Institute is supported by the «Ministère de l'Enseignement Supérieur et de la Recherche», the «Région Nord-Pas de calais» and the «Fonds Européen de Développement des Régions».

References

[1] F. Lin, Y. Zhang, L. Wang, Y. Zhang, D. Wang, M. Yang, J. Yang, B. Zhang, Z. Jiang, C. Li, Applied Catalysis B: Environmental. 127 (2012) 363-370.

[2] D. Valencia, T. Klimova, Applied Catalysis B: Environmental. 129 (2013) 137-145.

[3] International Energy Outlook 2019 with projections to 2050, 2019. https://www.eia.gov/outlooks/ieo/

[4] C. Perego, A. Bosetti, Microporous and Mesoporous Materials. 144 (2011) 28-39.

[5] H. Lü, W. Ren, W. Liao, W. Chen, Y. Li, Z. Suo, Applied Catalysis B: Environmental. 138-139 (2013) 79-83.

[6] C. Thomazeau, C. Geantet, M. Lacroix, M. Danot, V. Harle, P. Raybaud, Applied Catalysis A: General. 322 (2007) 92-97.

[7] P.J. Vázquez-Salas, R. Huirache-Acuña, T.A. Zepeda, G. Alonso-Núñez, R. Maya-Yescas, N. Mota, B. Pawelec, Catalysis Today. 305 (2018) 65-74.

[8] L. van Haandel, M. Bremmer, P.J. Kooyman, J.A. Rob van Veen, T. Weber, E.J.M. Hensen, ACS Catalysis. 5 (2015) 7276-7287.

[9] S. Sigurdson, V. Sundaramurthy, A.K. Dalai, J. Adjaye, Journal of Molecular Catalysis A: Chemical. 291 (2008) 30-37.

[10] G. An, C. Liu, C. Xiong, C. Lu, Petroleum Science and Technology. 30 (2012) 1599-1608

[11] J. A. Mendoza-Nieto, O. Vera-Vallejo, L. Escobar-Alarcón, D. Solís-Casados, T. Klimova, Fuel. 110 (2013) 268-277.

[12] R. Huirache-Acuña, B. Pawelec, C.V. Loricera, E.M. Rivera-Mu˜noz, R. Nava, B. Torres, J.L.G. Fierro, Applied Catalysis B: Environmental. 125 (2012) 473-485.

[13] P. Nikulshin, A. Mozhaev, C. Lancelot, P. Blanchard, E. Payen, C. Lamonier, Comptes Rendus Chimie. 19 (2016) 1276-1285.

[14] R. Shafi, M.R.H. Siddiqui, G.J. Hutchings, E.G. Derouane, I.V. Kozhevnikov, Applied Catalysis A: General. 204 (2000) 251-256.

[15] P. Blanchard, C. Lamonier, A. Griboval, E. Payen, Applied Catalysis A: General. 322 (2007) 33-45.

[16] C.I. Cabello, F.M. Cabrerizo, A. Alvarez, H.J. Thomas, Journal of Molecular Catalysis A: Chemical. 186 (2002) 89-100.

[17] C. Lamonier, C. Martin, J. Mazurelle, V. Harlé, D. Guillaume, E. Payen, Applied Catalysis B: Environmental. 70 (2007) 548-556.

[18] M. Nikulshina, A. Mozhaev, C. Lancelot, M. Marinova, P. Blanchard, E. Payen, C. Lamonier, P. Nikulshin, Applied Catalysis B: Environmental. 224 (2018) 951-959.

[19] M. Nikulshina, P. Blanchard, A. Mozhaev, C. Lancelot, A. Griboval-Constant, M. Fournier, C. Lamonier, Catalysis Science & Technology. 8 (2018) 5557-5572.

[20] M. Nikulshina, A. Mozhaev, C. Lancelot, P. Blanchard, M. Marinova, C. Lamonier, P. Nikulshin, Catalysis Today 329 (2019) 24-34.

[21] M.T. Pope, Heteropoly and Isopoly Oxometalates, Springer-Verlag, Berlin, 1983.

[22] SAINT: Area-Detector Integration Software. Madison: Siemens Industrial Automation, Inc., 1996

[23] G. Sheldrix, SADABS: Area Detector Absorption Correction, Madison, WI, 1996

[24] L. Palatinus, G. Chapuis, Journal of Applied Crystallography. 40 (2007) 786-790.

[25] V. Petricek, M. Dusek, L. Palatinus, Kristallografiya. 229 (2014) 345-352.

[26] S. Kasztelan, H. Toulhoat, J. Grimblot, J.P. Bonnelle, Applied Catalysis. 13 (1984) 127-159.

[27] A.V. Mozhaev, P.A. Nikulshin, Al.A. Pimerzin, K.I. Maslakov, A.A. Pimerzin, Catalysis Today. 271 (2016) 80-90.

[28] A. Cordova, P. Blanchard, C. Lancelot, G. Frémy, C. Lamonier, ACS Catalysis. 5 (2015) 2966-2981.

[29] C. Rocchiccioli-Deltcheff, M. Fournier, R. Franck, R. Thouvenot, Inorganic Chemistry. 22 (1983) 207-216.

[30] C. Rocchiccioli-Deltcheff, R. Thouvenot, R. Franck, Spectrochimica Acta Part A. 32 (1976) 587-597.

[31] A.J. Bridgeman, Chemical Physics. 287 (2003) 55-69.

[32] A.J. Bridgeman, Chem. Eur. J. 10 (2004) 2935-2941

[33] L.C. Teague, D. Chen, J.J. Boland, Journal of Physical Chemistry B. 108 (2004) 7827-7830.

[34] M. Muñoz, C.I. Cabello, I.L. Botto, G. Minelli, M. Capron, C. Lamonier, E. Payen, Journal of Molecular Structure. 841 (2007) 96-103.

[35] L. Catita, A.-A. Quoineaud, D. Espinat, C. Pichon, O. Delpoux, Applied Catalysis A: General. 547 (2017) 164-175.

[36] L. Le Bihan, P. Blanchard, M. Fournier, J. Grimblot, E. Payen, Journal of the Chemical Society, Faraday Transactions. 94 (1998) 937-940.

[37] X. Carrier, J.F. Lambert, M. Che, Journal of the American Chemical Society. 119 (1997) 10137-10146.

[38] P. Hartel, H. Rose, C. Dignes, Ultramicroscopy. 63 (1996) 93-114.

[39] M. Nikulshina, P. Blanchard, C. Lancelot, A. Griboval-Constant, M. Marinova, V. Briois, P. Nikulshin, C. Lamonier, Applied Catalysis B: Environmental. 269 (2020) 118766.

[40] R. Thomas, E.M. van Oers, V.H.J. de Beer, J. Medema, J.A. Moulijn, Journal of Catalysis. 76 (1982) 241-253.

[41] T.F. Hayden, J.A. Dumesic, R.D. Sherwood, R.T.K. Baker, Journal of Catalysis. 105 (1987) 299-318.

[42] E. Payen, R. Hubaut, S. Kasztelan, O. Poulet, J. Grimblot, Journal of Catalysis. 147 (1994) 123-132.

[43] R. Huirache-Acuña, B. Pawelec, E. M. Rivera-Muñoz, R. Guil-López, J. L. G. Fierro, Fuel. 198 (2017) 145–158.

[44] H. Wang, L. Ouyang, G. Zou, C. Sun, J. Hu, X. Xiao, L. Gao, ACS Catalysis. (2018) 1-22.

1

2

1 **Captions for Tables**

Table 1. Crystal data, data collection and structure refinement parameters for $H_4[SiMo_6W_6O_{40}]\cdot 36H_2O$ and $H_4[SiMo_9W_3O_{40}]$ $36H_2O$.

Table 2. Composition and textural characteristics of sulfided Mo(W) catalysts.

Table 3. Morphological characteristics of sulfided Mo(W) catalysts.

Table 4. Metal distribution for Mo and W species present at the surface of sulfided Mo(W) catalysts.

Table 5. Catalytic properties of supported Mo(W) catalysts in the hydrotreating of DBT and naphthalene.

2

3 **Captions for Figures**

Figure 1. IR-spectra for $SiMo_nW_{12-n}$HPAs.

Figure 2. Raman spectra for $SiMo_nW_{12-n}$HPAs.

Figure 3. Crystals and detailed heteropolyanion structures and formation of $H_4[SiMo_6W_6O_{40}]\cdot 36H_2O$ and $H_4[SiMo_9W_3O_{40}]$ $36H_2O$.

Figure 4. Raman spectra for oxidic MoW catalysts dried at 110 ºC.

Figure 5. HRTEM micrographs of sulfided MoW catalysts.

Figure 6. HAADF images of sulfided MoW catalysts.

* adapted from [20].

Figure 7. XPS Mo 3d and W 4f spectra recorded for sulfided MoW catalysts; in blue: $Mo(W)^{6+}$ oxide contributions; in pink: $Mo(W)S_xO_y$ contributions; in black: $Mo(W)S_2$ contributions: in green S contributions. (For interpretation of the references to color in this figure legend, the reader is referred to the web version of this article.)

Figure 8. Dependence of reaction rate constants in DBT HDS (a) and naphthalene HYD (b) on Mo/(Mo+W) atomic in MoW catalysts (circles correspond to mixed MoW catalysts prepared from mixed $SiMo_nW_{12-n}HPA$; squares are mixed Mo+W catalysts prepared from a mixture of $SiMo_{12}$ and $SiW_{12}HPA$). * adapted from [20].

Figure 9. Dependence of average stacking number on Mo/(Mo+W) ratio in MoW catalysts (circles correspond to mixed MoW catalysts prepared from mixed $SiMo_nW_{12-n}HPA$; squares are mixed Mo+W catalysts prepared from a mixture of $SiMo_{12}$ and $SiW_{12}HPA$).

Figure 10. Dependence of TOF_{edge} number in DBT HDS (a) and naphthalene HYD (b) on Mo/(Mo+W) atomic ratio in MoW catalysts; (circles correspond to mixed MoW catalysts prepared from mixed $SiMo_nW_{12-n}HPA$; squares are mixed Mo+W catalysts prepared from a mixture of $SiMo_{12}$ and $SiW_{12}HPA$; triangles are the additive quantities which were calculated using the values for monometallic Mo_{12}/Al_2O_3 and W_{12}/Al_2O_3).

Figure 11. Dependence of DBT HDS (a) and naphthalene HYD (b) rate constants on total number of edge sites

Figure 12. Relationships between sulfidation degree of Mo (W) in MoW/Al_2O_3 catalysts, their HDS activity and Mo/(Mo+W) atomic ratio. *The active phase models are based on HAADF..*

1

Table 1. Crystal data, data collection and structure refinement parameters for

$H_4[SiMo_6W_6O_{40}]\cdot 36H_2O$ and $H_4[SiMo_9W_3O_{40}]\ 36H_2O$

Crystal data		
Cluster formula	$H_4[SiMo_6W_6O_{40}]$	$H_4[SiMo_9W_3O_{40}]$
Crystal symmetry	Tetragonal	
Space group	$P\text{-}42_1c$	
Working temp. (K)	100	293
Unit cell (Å)	a = 12.732(2) c = 18.0525(6)	12.7447(3) 18.0632(9)
Volume ($Å^3$)	2926.38	2933.96
Z, Mw	2, 2994.8	2, 2761.02
Calculated density (g/cm^3)	3.40	3.12
Data collection		
Equipment	Bruker Apex Duo	
Radiation MoKα (Å)	0.71073	
Scan mode	ω/φ - scan	
Recorded angular range θ (°)	1.96 – 33.13	1.96 – 31.69
Recording reciprocal space	$-15 \le h \le 19$	$-18 \le h \le 18$
	$-19 \le k \le 16$	$-18 \le k \le 18$
	$-27 \le l \le 27$	$-26 \le l \le 26$
N. ind. Ref.	2656	2672
N. ind. Ref. [I>3σ(I)]	2465	2222
μ (cm^{-1}) (λ = MoKα)	131.1	78.8
Absorption correction	analytical (Sadabs)	
R merging factor (%)	4.12	4.22
Refinement parameters		
Software	Jana 2000	
Number of refined parameters	106	107
R_1 (F) all , [I>3σ(I)] $= \Sigma \lvert \lvert F_O \rvert - \lvert F_C \rvert \rvert / \Sigma \lvert F_O \rvert$ (%)	3.62, 4.01	3.45, 4.67
wR_2 (F^2) all, [I>3σ(I)] $= \left[\Sigma w \left(F_O^2 - F_C^2 \right)^2 / \Sigma w \left(F_O^2 \right) \right]^{1/2}$ (%)	3.85, 4.14	5.27, 5.21
Weight	unit	$1/(\sigma^{2\wedge}(F)+0.0001F^2)$
Isotropic secondary extinction	none	none
Max / Min Δρ $e/Å^3$	-1.37/1.95	-1.05/1.81

Table 2. Composition and textural characteristics of sulfided Mo(W) catalysts.

Catalyst	d(Me) at/nm^2	Content (wt. %)		Textural characteristics		
		Mo	W	S_{BET}[a] (m^2 g^{-1})	V_p[b] (cm^3 g^{-1})	D[c] (nm)
Mo_{12}/Al_2O_3*	3.9	18.0	-	215	0.53	7.6
Mo_9W_3/Al_2O_3		13.1	7.1	204	0.56	7.7
Mo_9+W_3/Al_2O_3				210	0.59	7.5
Mo_6W_6/Al_2O_3		8.5	13.8	191	0.58	7.9
Mo_6+W_6/Al_2O_3				204	0.59	7.8
Mo_3W_9/Al_2O_3*		4.2	20.1	210	0.53	7.6
Mo_3+W_9/Al_2O_3*				206	0.53	7.6
W_{12}/Al_2O_3*		-	26.2	208	0.54	7.6

S_{BET} is the surface area, V_p is the pore volume, and D is the pore diameter.

* adapted from [20]

Table 3. Morphological characteristics of sulfided Mo(W) catalysts.

Catalyst	Average length $\bar{L}$ (nm)	Average stacking number $\bar{N}$	Dispersion of MoS_2 particles D	Distribution of slab length (rel. %)					Distribution of stacking number (rel. %)			
				<2 nm	2-4 nm	4-6 nm	6-8 nm	>8 nm	1	2	3	>4
Mo_{12}/Al_2O_3	3.8	1.2	0.31	3	61	30	5	1	79	18	2	1
Mo_9W_3/Al_2O_3	4.0	1.5	0.29	2	49	40	8	1	57	37	4	2
Mo_9+W_3/Al_2O_3	3.6	1.2	0.32	6	62	29	2	1	82	15	2	1
Mo_6W_6/Al_2O_3	3.9	1.4	0.30	3	57	34	5	1	70	24	5	1
Mo_6+W_6/Al_2O_3	3.8	1.3	0.31	3	58	31	6	2	73	24	2	1
Mo_3W_9/Al_2O_3	3.8	2.0	0.34	4	56	36	3	1	34	42	14	10
Mo_3+W_9/Al_2O_3	3.5	2.3	0.29	6	68	23	2	1	29	29	30	12
W_{12}/Al_2O_3	4.2	1.2	0.28	2	46	42	8	2	84	14	2	-

[a] MoS_2 dispersion calculated from HRTEM results.

Table 4. Metal distribution for Mo and W species present at the surface of sulfided Mo(W) catalysts.

Catalyst	Mo percentage (rel. %)			W percentage (rel. %)			Number of edge sites (10^{20} at g^{-1})		
	MoS_2	MoS_xO_y	Mo^{6+}	WS_2	WS_xO_y	W^{6+}	Mo_{edge}^{IV}	W_{edge}^{IV}	$\sum Mo_{edge}^{IV} + W_{edge}^{IV}$
Mo_{12}/Al_2O_3*	70	15	15	-	-	-	0.88	-	0.88
Mo_9W_3/Al_2O_3	91	7	2	85	3	12	0.82	0.60	1.42
Mo_9+W_3/Al_2O_3	83	11	6	71	6	23	0.87	0.59	1.46
Mo_6W_6/Al_2O_3	91	7	1	76	5	19	0.61	0.80	1.40
Mo_6+W_6/Al_2O_3	81	16	3	64	18	19	0.63	0.80	1.43
Mo_3W_9/Al_2O_3*	89	2	9	58	8	34	0.23	0.94	1.17
Mo_3+W_9/Al_2O_3*	90	8	2	77	11	12	0.48	0.74	1.22
W_{12}/Al_2O_3*	-	-	-	51	16	33	-	0.98	0.98

* - Adapted from [20]

Table 5. Catalytic properties of supported MoW catalysts in the hydrotreating of DBT and naphthalene.

Catalyst	Conversion (%)		Reaction rate constant ($\times 10^5$ mol h^{-1} g^{-1})		$S_{HYD/DDS}$
	DBT HDS	Naphthalene HYD	k_{HDS}	k_{HYD}	
Mo_{12}/Al_2O_3*	51.9	40.5	45	157	1.73
Mo_9W_3/Al_2O_3	59.2	55.2	55	244	2.83
Mo_9+W_3/Al_2O_3	44.3	39.6	36	153	2.51
Mo_6W_6/Al_2O_3	61.3	57.3	59	258	3.16
Mo_6+W_6/Al_2O_3	47.6	42.2	40	166	2.33
Mo_3W_9/Al_2O_3*	52.9	47.5	46	195	3.18
Mo_3+W_9/Al_2O_3*	32.1	27.3	24	97	1.76
W_{12}/Al_2O_3*	22.2	23.8	15	82	2.61

* - Adapted from [20]

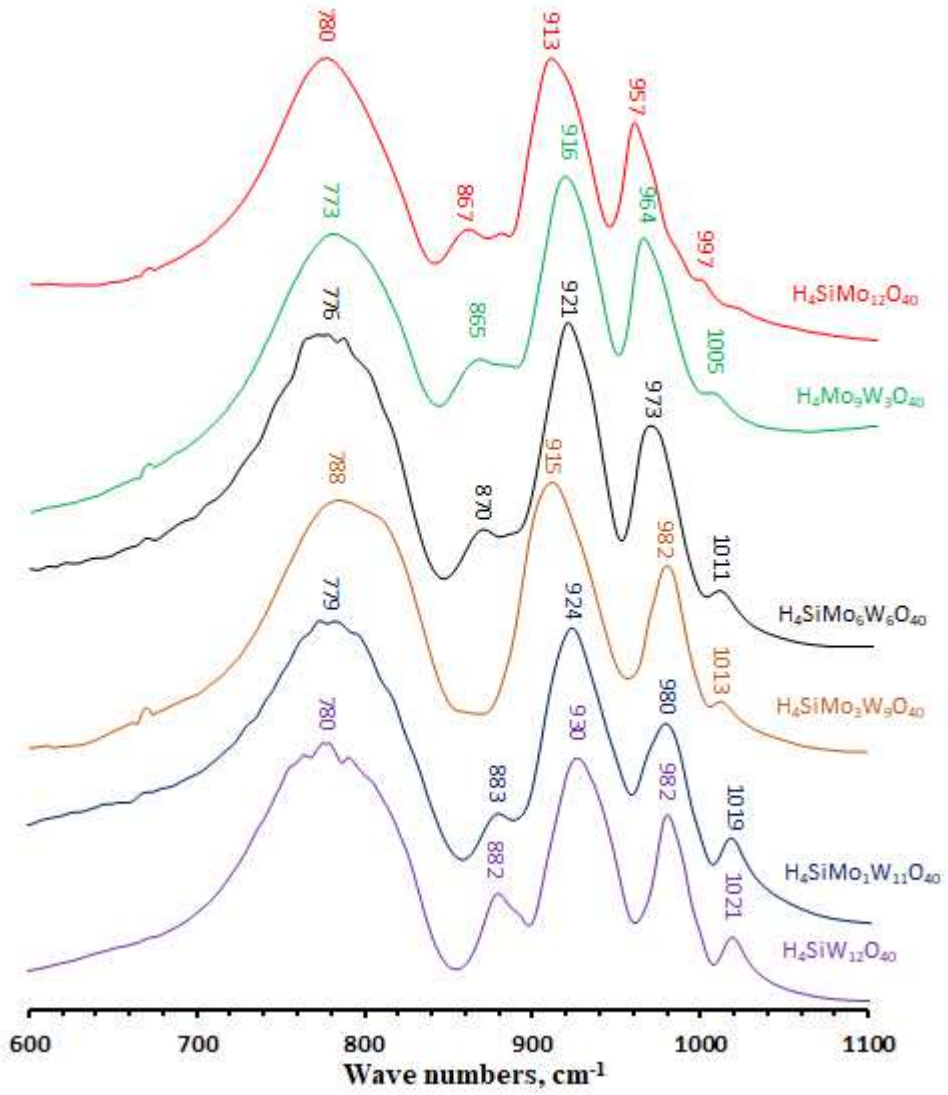

Fig. 1. IR-spectra for $SiMo_nW_{12-n}$HPAs.

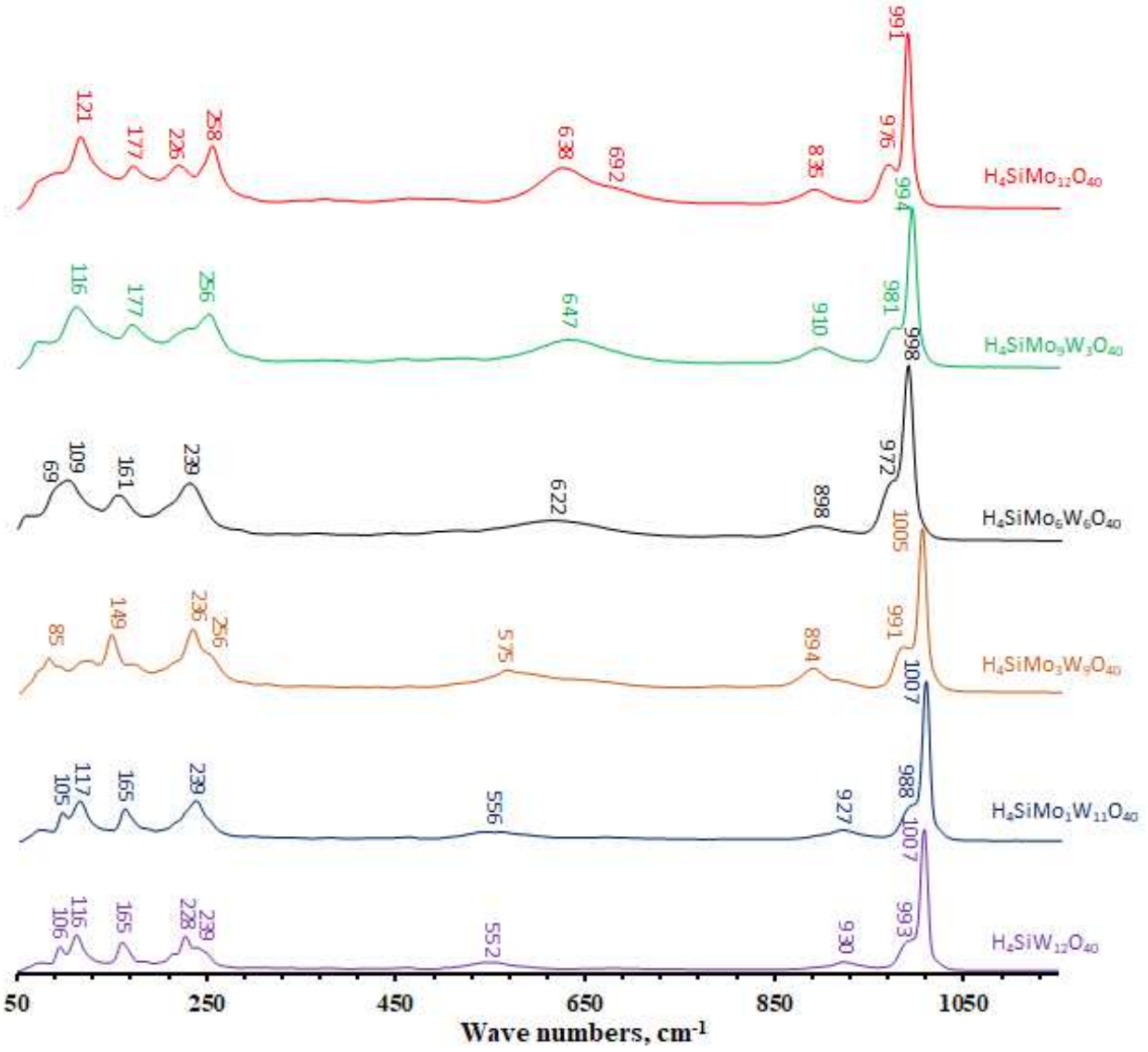

Fig. 2. Raman spectra for $SiMo_nW_{12-n}$HPAs.

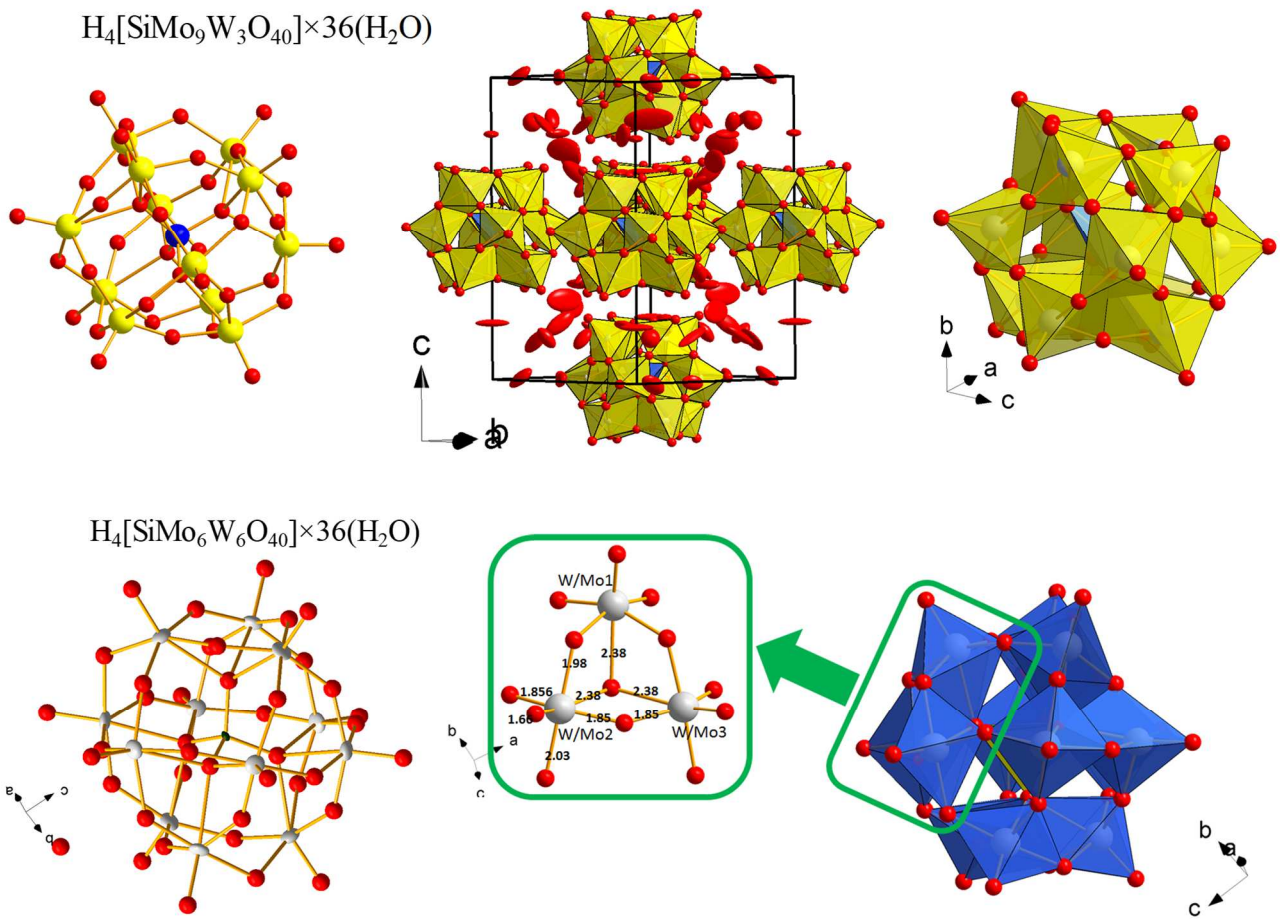

Fig. 3. Crystals and detailed heteropolyanion structures and formation of $H_4[SiMo_6W_6O_{40}]\cdot 36H_2O$ and $H_4[SiMo_9W_3O_{40}]\ 36H_2O$

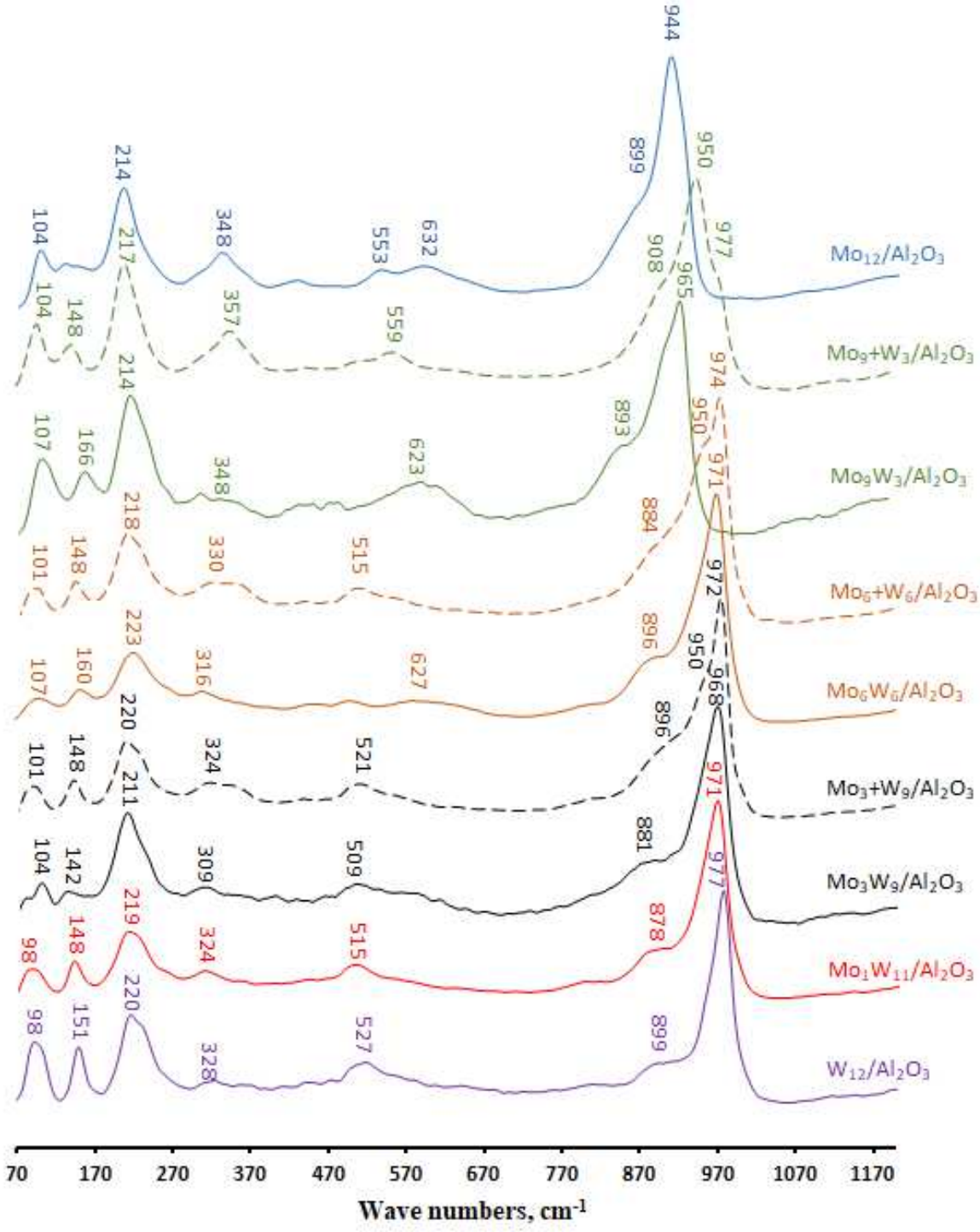

Fig. 4. Raman spectra for oxidic MoW catalysts dried at 110 ºC.

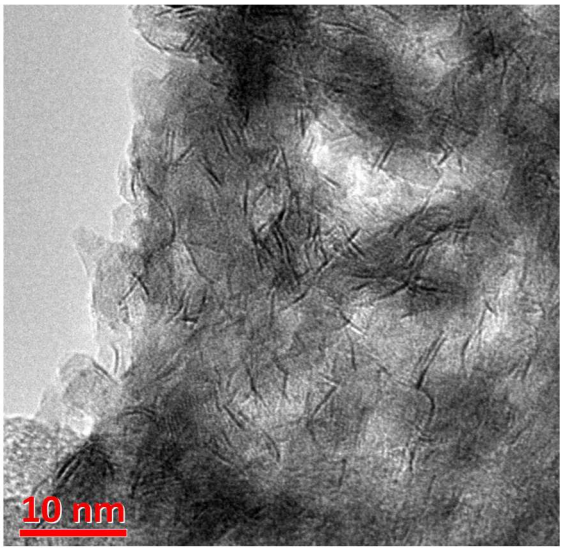

Mo_6W_6/Al_2O_3

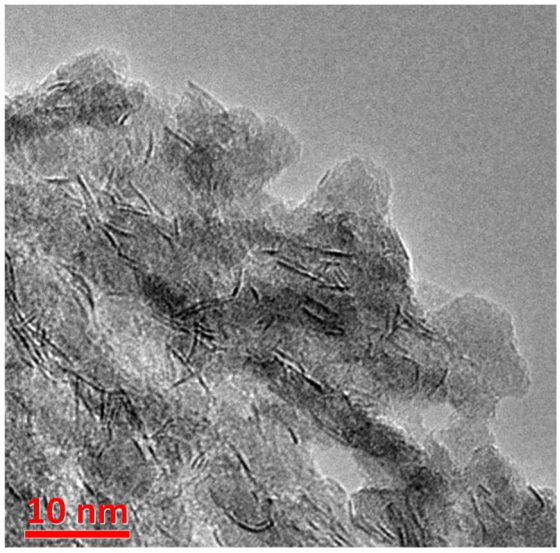

Mo_6+W_6/Al_2O_3

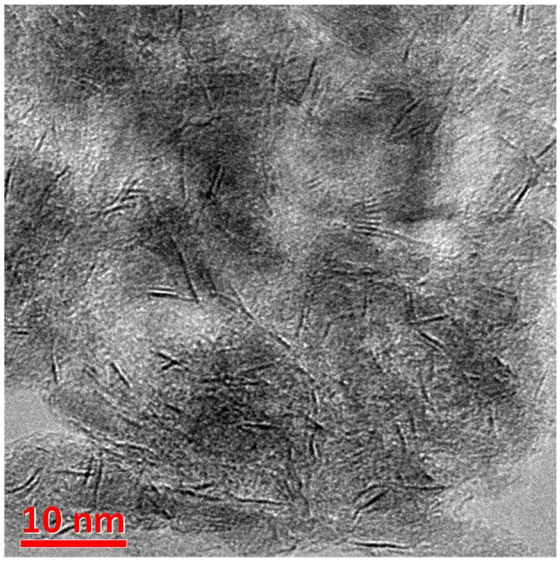

Mo_9W_3/Al_2O_3*

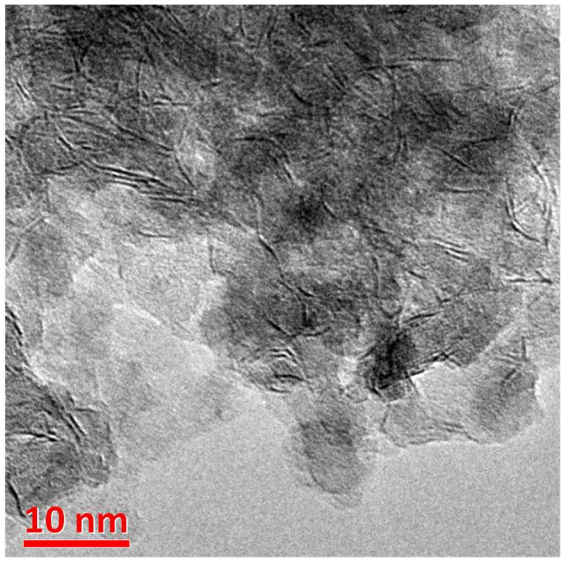

Mo_9+W_3/Al_2O_3*

Fig. 5. HRTEM micrographs of sulfided MoW catalysts.

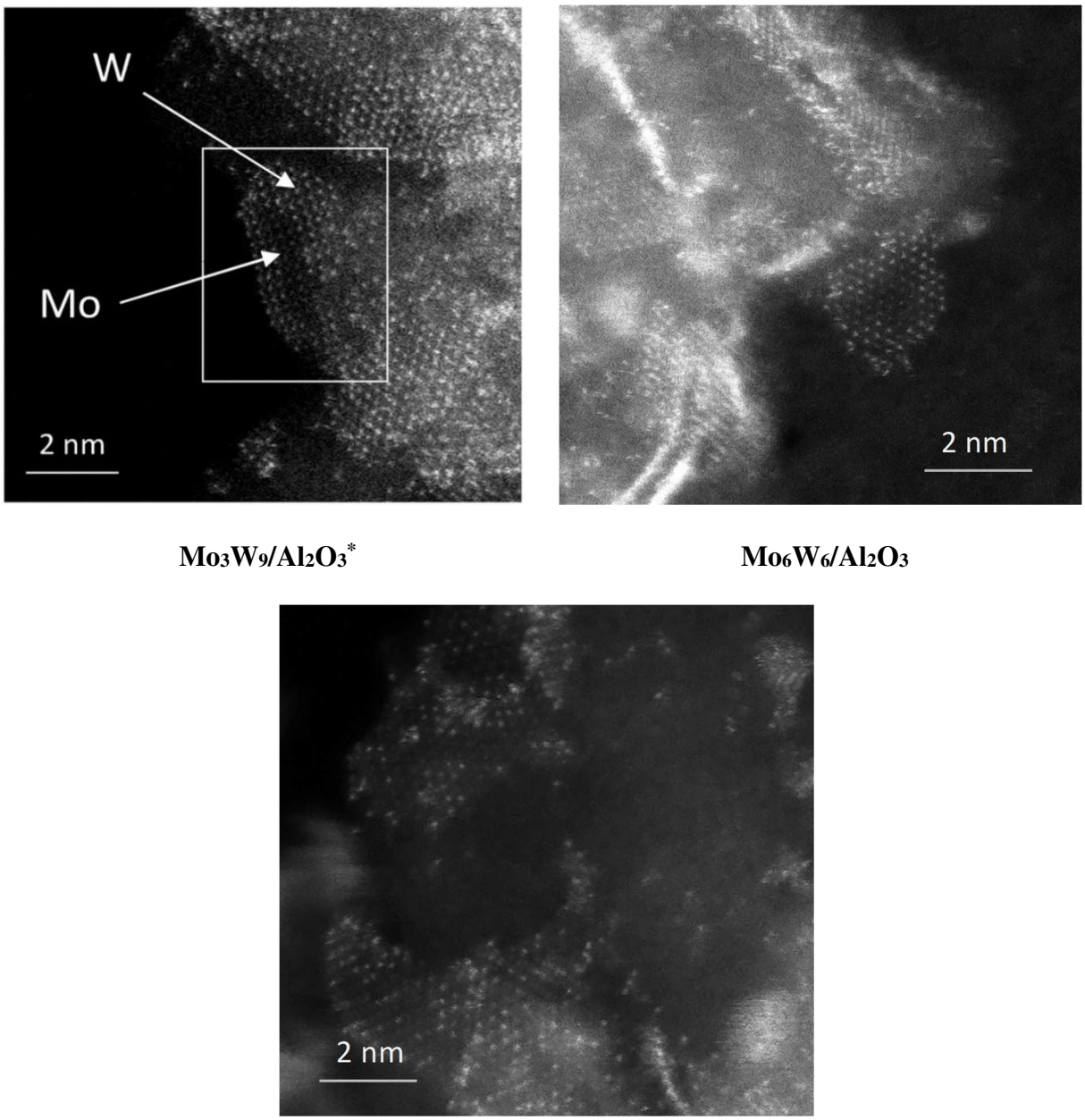

Mo_3W_9/Al_2O_3* **Mo_6W_6/Al_2O_3**

Mo_9W_3/Al_2O_3

Fig. 6. HAADF images of sulfided MoW catalysts.

* adapted from [20].

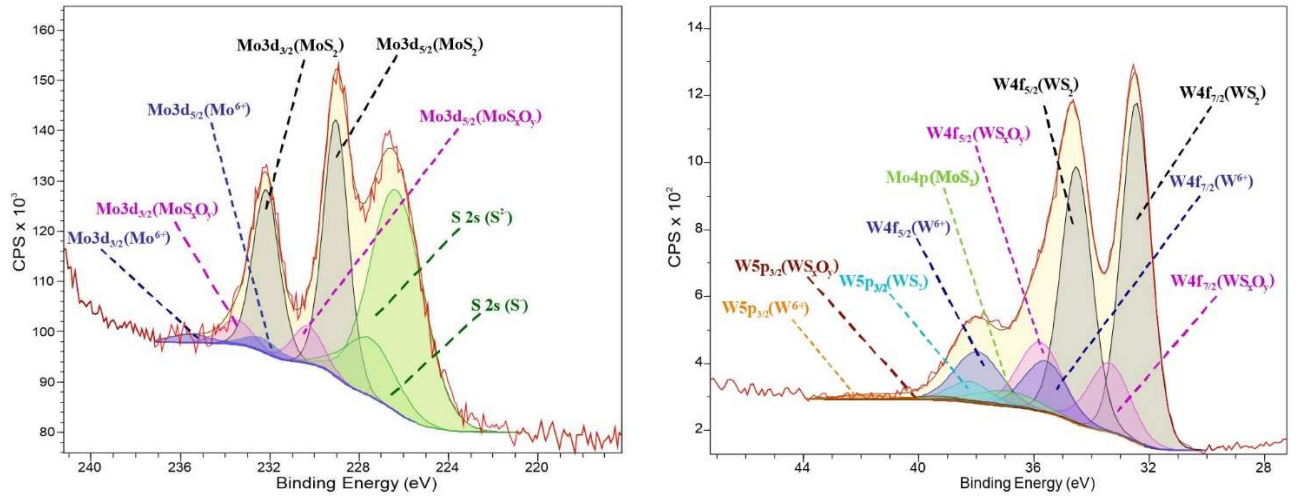

Mo_3W_9/Al_2O_3

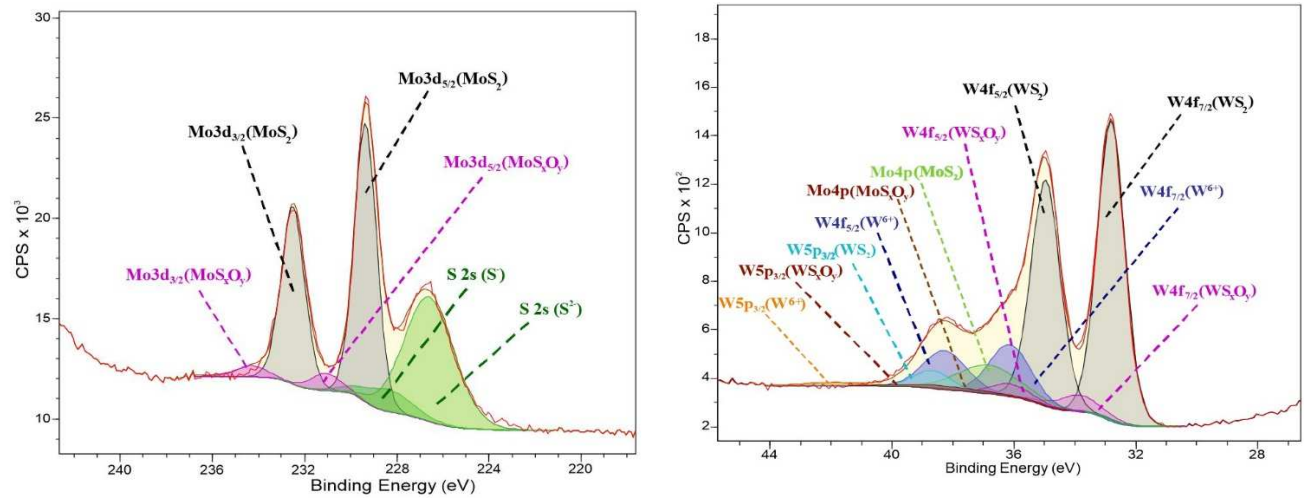

Mo_6W_6/Al_2O_3

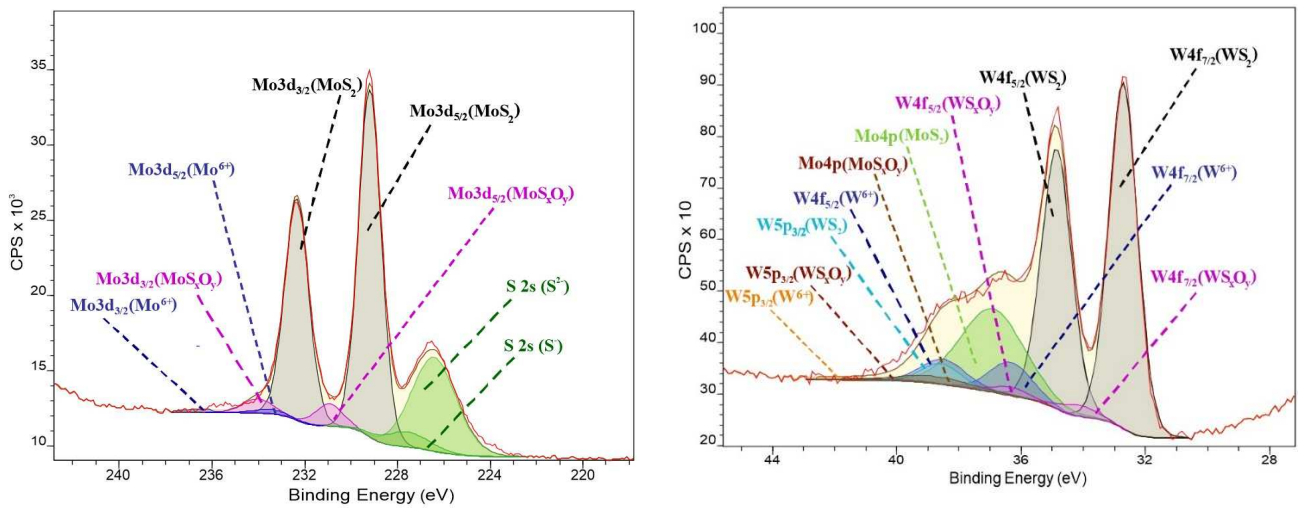

Mo_9W_3/Al_2O_3

Fig. 7. XPS Mo 3d and W 4f spectra recorded for sulfided MoW catalysts; in blue: $Mo(W)^{6+}$ oxide contributions; in pink: $Mo(W)S_xO_y$ contributions; in black: $Mo(W)S_2$ contributions: in green S contributions. (For interpretation of the references to color in this figure legend, the reader is referred to the web version of this article.)

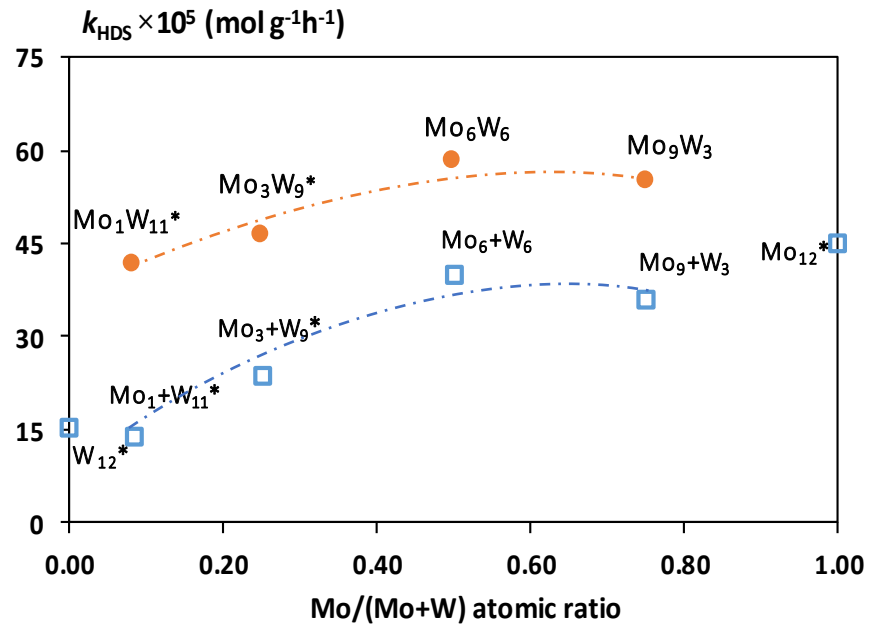

(a)

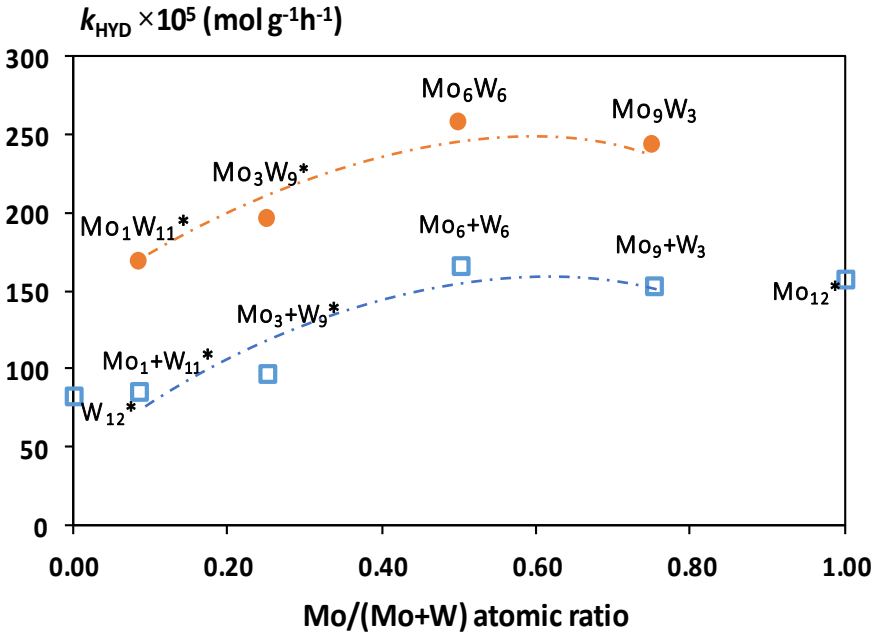

(b)

Fig. 8. Dependence of reaction rate constants in DBT HDS (a) and naphthalene HYD (b) on Mo/(Mo+W) atomic in MoW/Al_2O_3 catalysts (circles correspond to mixed MoW catalysts prepared from mixed $SiMo_nW_{12-n}HPA$; squares are mixed Mo+W catalysts prepared from a mixture of $SiMo_{12}$ and $SiW_{12}HPA$). * adapted from [20].

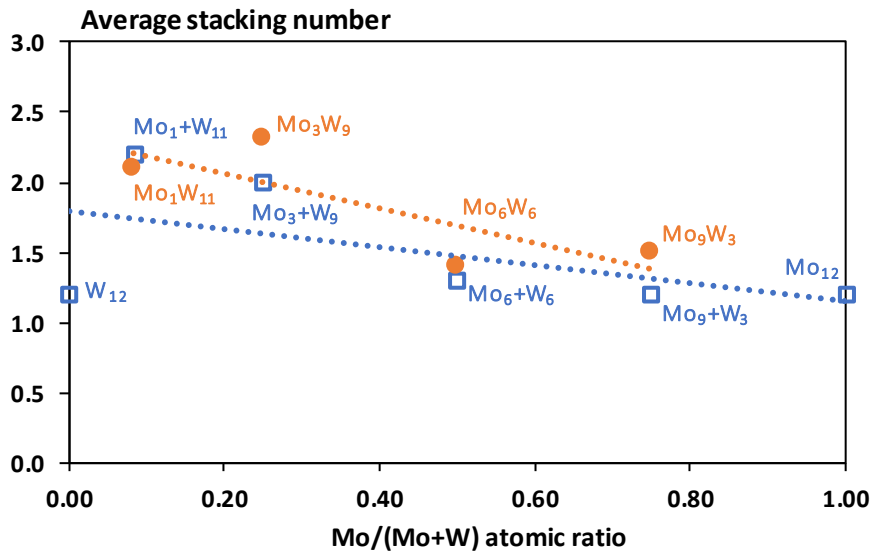

Fig. 9. Dependence of average stacking number on Mo/(Mo+W) ratio in MoW catalysts (circles correspond to mixed MoW/Al_2O_3 catalysts prepared from mixed $SiMo_nW_{12-n}$HPA; squares are mixed Mo+W/Al_2O_3 catalysts prepared from a mixture of $SiMo_{12}$ and SiW_{12}HPA).

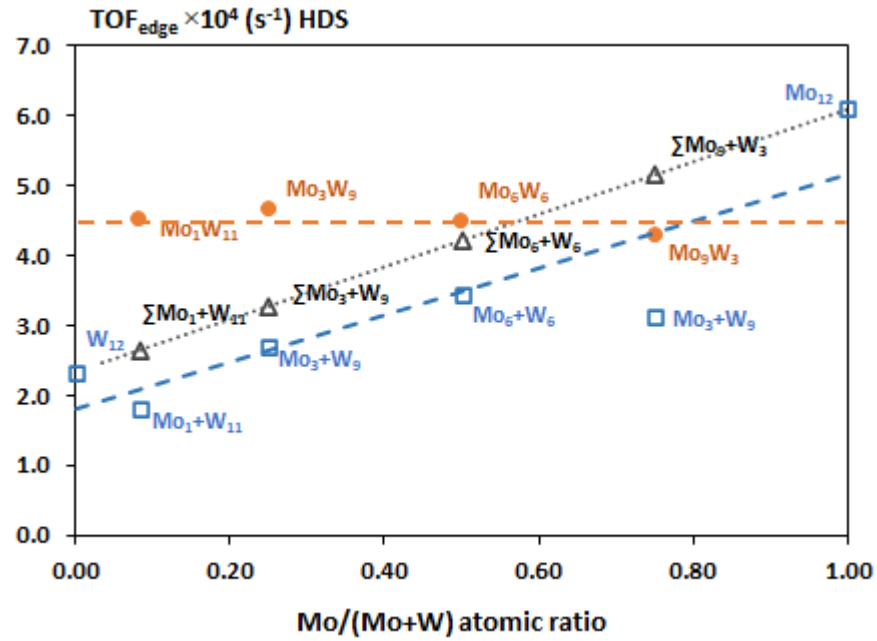

(a)

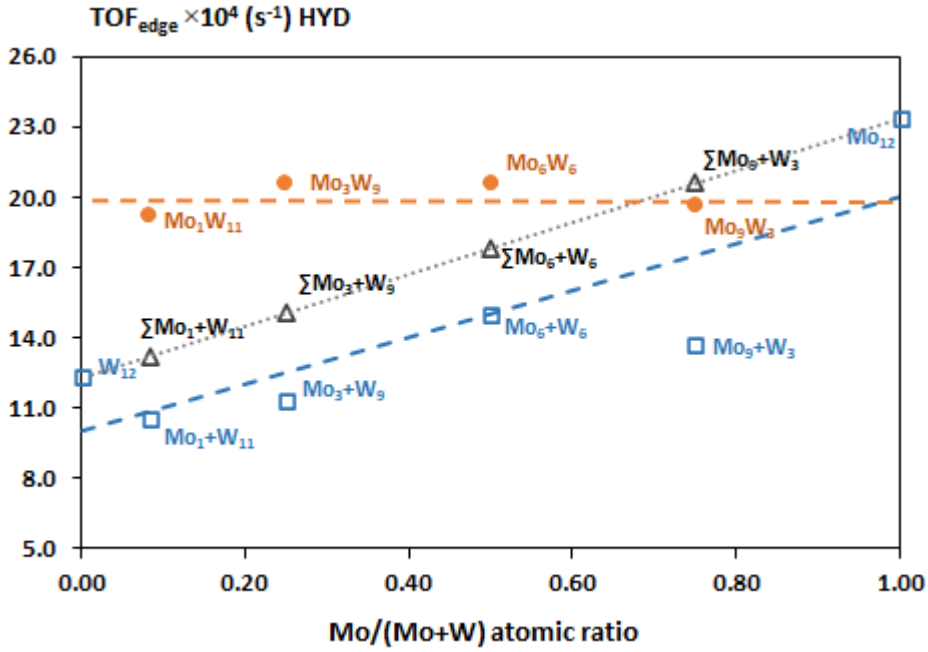

(b)

Fig. 10. Dependence of TOF_{edge} number in DBT HDS (a) and naphthalene HYD (b) on Mo/(Mo+W) atomic ratio in MoW catalysts; (circles correspond to mixed MoW catalysts prepared from mixed $SiMo_nW_{12-n}HPA$; squares are mixed Mo+W catalysts prepared from a mixture of $SiMo_{12}$ and $SiW_{12}HPA$; triangles are the additive quantities which were calculated using the values for monometallic Mo_{12}/Al_2O_3 and W_{12}/Al_2O_3).

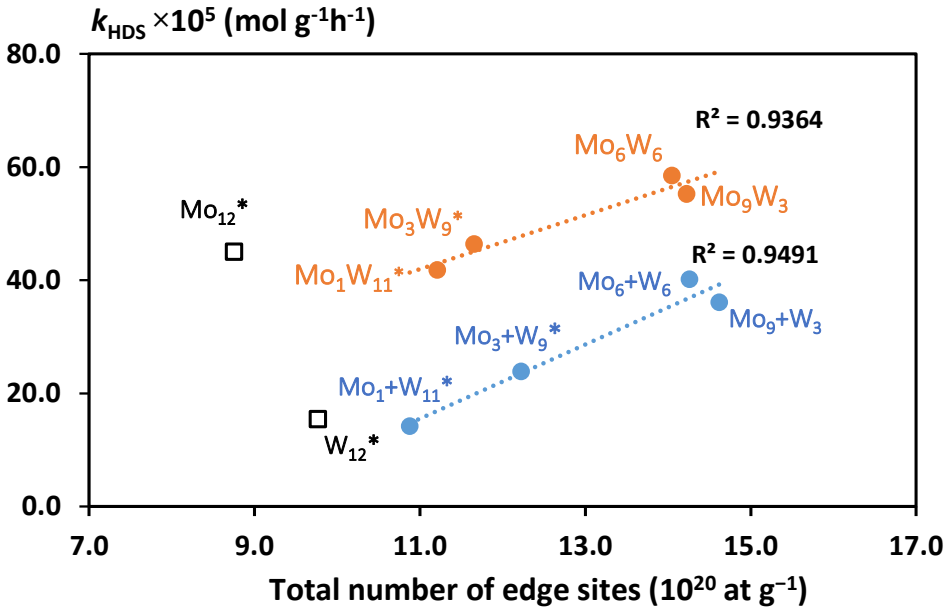

(a)

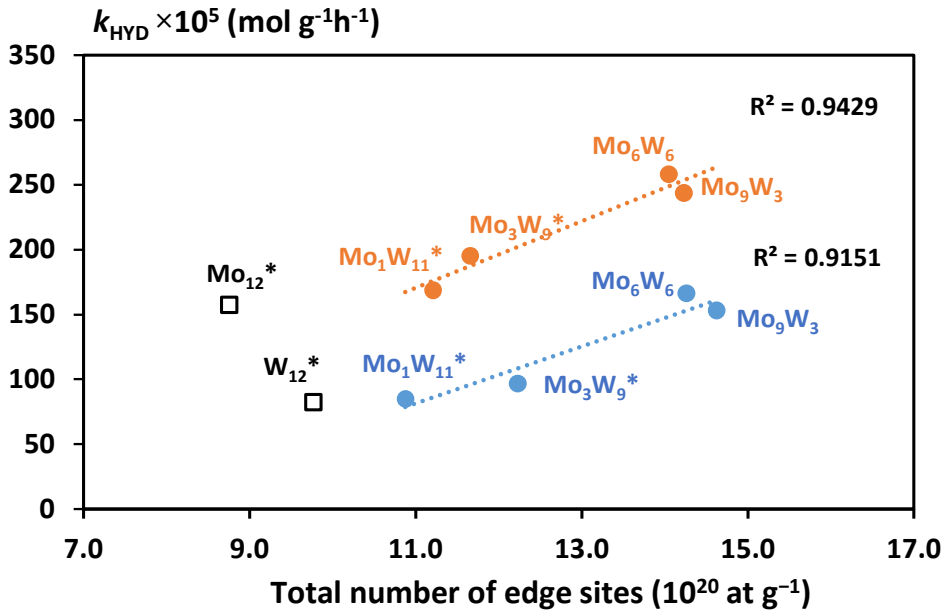

(b)

Fig. 11. Dependence of DBT HDS (a) and naphthalene HYD (b) rate constants on total number of edge sites

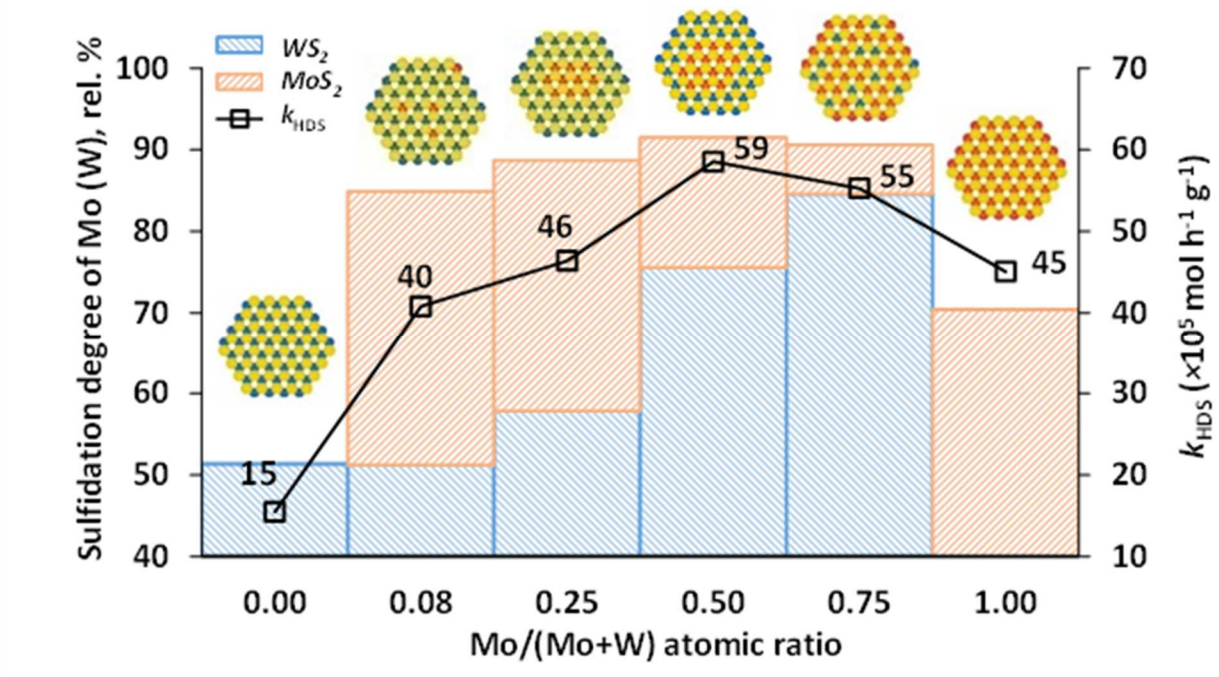

Fig. 12. Relationships between sulfidation degree of Mo (W) in MoW/Al_2O_3 catalysts, their HDS activity and Mo/(Mo+W) atomic ratio. *The active phase models are based on HAADF.*